
LAW OF VISION REPRESENTATION IN MLLMs

Shijia Yang¹

Bohan Zhai

Quanzeng You

Jianbo Yuan

Hongxia Yang

Chenfeng Xu²

¹STANFORD UNIVERSITY ²UC BERKELEY

ABSTRACT

We present the ‘‘Law of Vision Representation’’ in multimodal large language models (MLLMs). It reveals a strong correlation between the combination of cross-modal alignment, correspondence in vision representation, and MLLM performance. We quantify the two factors using the cross-modal **Alignment** and **Correspondence** score (AC score). Through extensive experiments involving thirteen different vision representation settings and evaluations across eight benchmarks, we find that the AC score is linearly correlated to model performance. By leveraging this relationship, we are able to identify and train the optimal vision representation only, which does not require finetuning the language model every time, resulting in a 99.7% reduction in computational cost. The code is available at https://github.com/bronyayang/Law_of_Vision_Representation_in_MLLMs.

1 INTRODUCTION

Current multimodal large language models (MLLMs) (Chen et al., 2024a; Liu et al., 2024e;d) have achieved remarkable advancements by integrating pretrained vision encoders with powerful language models (Touvron et al., 2023; Zheng et al., 2023). As one of the core components of a general MLLM, the vision representation is critical. Many researchers have utilized CLIP (Radford et al., 2021) as the primary image feature encoder, but its limitations are increasingly noticeable (Tong et al., 2024b; Geng et al., 2023; Yao et al., 2021). As a result, alternative vision representation and the combination of multiple vision encoders are being actively explored (Tong et al., 2024a; Lin et al., 2023).

Despite this growing attention, the selection of vision representation has largely been empirical. Researchers typically test a set of vision representations on a specific MLLM and choose the one that yields the highest performance on benchmark tasks. This approach, however, is constrained by the number of representations tested and does not address the underlying factors that make certain feature representations perform better than others. As a result, the optimal vision representation for a specific MLLM is often determined by empirical performance rather than a deep understanding of the features that contribute to success. The question of what fundamentally makes a feature representation achieve the highest performance remains largely unanswered.

To address this gap in understanding what makes a vision representation optimal for MLLMs, we propose the **Law of Vision Representation in MLLMs**. It aims to explain the key factors of vision representation that impact MLLM benchmarks performance. Our findings reveal that *the cross-modal Alignment and Correspondence (AC) of the vision representation are strongly correlated with model performance*. Specifically, an increase in the AC of the selected vision representation leads to improved model performance. To quantify this relationship, we define an **AC score** that measures cross-modal alignment and correspondence in vision representation. The AC score and model performance exhibit a linear relationship, with a coefficient of determination of 95.72%.

Furthermore, the Law of Vision Representation guides the selection of an optimal vision representation for MLLMs. Originally, this process was extremely costly because even subtle changes in

vision encoding methods—such as switching encoder types, altering image resolution, or testing feature combinations—require finetuning the language model (Lin et al., 2024). For example, using a top data-efficient MLLM pipeline with a 7B language model requires 3,840 NVIDIA A100 GPU hours to test the 10 encoders used in this study, amounting to a cost of approximately \$20,000¹. Testing additional encoders leads to a linear increase in cost. Moreover, the recent trend of feature combination, which often results in better performance, necessitates combinatorial testing of vision encoders. Testing all possible combinations of 10 encoders results in 1023 combinations, exponentially increasing the cost and energy consumption. This process consumes approximately 100,000 kilowatt-hours², enough to drive an electric vehicle around the Earth 13 times.

Thus, we are the first to propose a policy, **AC policy**, that selects the optimal vision representation using AC scores within the desired search space. Unlike traditional methods that rely on benchmarking performance, the AC policy enables the expansion of the search space—allowing for an increased number of vision representations to be considered—without incurring additional costs. We demonstrate that this approach enhances both accuracy and efficiency compared to randomly searching for the optimal representation. The policy successfully identifies the optimal configuration among the top three choices in 96.6% of cases, with only three language model finetuning across a 13-setting search space.

2 RELATED WORKS

2.1 VISION FOR MLLMs

Recent studies have explored various vision representations in MLLMs (Beyer et al., 2024; Ge et al., 2024; Liu et al., 2024e; Wang et al., 2024; Sun et al., 2023; Luo et al., 2024). Interestingly, some findings indicate that relying solely on encoders outside of the CLIP family (Cherti et al., 2023; Zhai et al., 2023b; Li et al., 2022), such as DINOv2 (Oquab et al., 2023) and Stable Diffusion (Rombach et al., 2021), often leads to lower performance scores (Karamchetti et al., 2024; Tong et al., 2024a). However, combining features from these encoders with CLIP features—such as concatenating image embeddings in the token or channel dimension—significantly enhances performance beyond using CLIP alone (Tong et al., 2024a;b; Liu et al., 2024c; Kar et al., 2024). Researchers intuitively suggest that these additional encoders provide superior detail-oriented capabilities, but no studies have thoroughly analyzed the underlying causes of the performance change (Wei et al., 2023; Lu et al., 2024). This suggests that the attributes of an optimal vision representation remain not fully understood.

2.2 CROSS-MODAL ALIGNMENT

Cross-modal alignment refers to the alignment between image and text feature spaces (Duan et al., 2022). This concept emerged with the introduction of text-image contrastive learning (Radford et al., 2021; Jia et al., 2021). Although current MLLMs utilize contrastively pretrained image encoders, the challenge of achieving effective alignment persists (Ye et al., 2024; Zhai et al., 2023a; Woo et al., 2024). Despite efforts to critique the limitations of CLIP family representations and explore alternative vision representations, many approaches continue to rely on contrastively pretrained encoders or adding contrastive loss without fully eliminating them (Zhang et al., 2024a; Lu et al., 2024; Tong et al., 2024a;b; Liu et al., 2024b). In our work, we point out that alignment in vision representation is essential for improved model performance and is crucial for data efficiency. Without pre-aligned vision representations, extensive data pretraining is required to achieve cross-modal alignment within the language model (Ge et al., 2024; Chen et al., 2024b; Li et al., 2024b).

2.3 VISUAL CORRESPONDENCE

Visual correspondence is a fundamental component in computer vision, where accurate correspondences can lead to significant performance improvements in tasks, such as image detection (Xu et al., 2024; Nguyen & Meunier, 2019), visual creation (Tang et al., 2023; Zhang et al., 2024b), and MLLMs (Liu et al., 2024a), etc. Correspondences are typically categorized into semantic- and

¹<https://replicate.com/pricing>

²<https://www.nvidia.com/content/dam/en-zz/Solutions/Data-Center/a100/pdf/nvidia-a100-datasheet.pdf>

geometric-correspondences. Semantic correspondences (Zhang et al., 2024b; Min et al., 2019) involve matching points that represent the same semantic concept not necessarily representing the same instance. Geometric correspondences (Sarlin et al., 2020; Lindenberger et al., 2023), on the other hand, require matching the exact same point across images, which is often crucial for low-level vision tasks, such as pose estimation (Sarlin et al., 2020; Lindenberger et al., 2023; Zhang & Vela, 2015), and SLAM tasks, etc.

Several studies have pointed out that the CLIP family’s vision representation “lacks visual details” (Lu et al., 2024; Tong et al., 2024b; Ye et al., 2024). We explain this observation through the concept of correspondence. Current multi-modal large language models (MLLMs) convert images into embeddings, with each embedding representing a patch of the image. Image features with high correspondence increase the similarity within internal image patches on similar semantics, thereby enabling the retrieval of more detailed information.

3 LAW OF VISION REPRESENTATION IN MLLMs

We introduce the Law of Vision Representation in Multimodal Large Language Models (MLLMs). It states that the performance of a MLLM, denoted as Z , can be estimated by two factors: cross-modal alignment (A) and correspondence (C) of the vision representation, assuming vision representation is the sole independent variable while other components (e.g., language model and alignment module) remain fixed. This relationship can be expressed as:

$$Z \propto f(A, C) \quad (1)$$

where f is a linear function on second-degree polynomial transformations of A and C .

3.1 THEORETICAL JUSTIFICATION

In this section, we theoretically analyze how an increase in A and C leads to improved model performance. When a vision representation demonstrates high cross-modal alignment and accurate correspondence, the MLLM exhibits the following desired properties:

- *When training a MLLM, if the vision representation is closely pre-aligned with the language distribution, the pretrained language model requires less computational effort to bridge the gap between different modalities during finetuning.* In Section A.1, we provide theoretical justification that finetuning on well-aligned multimodal data is about equivalent to finetuning on text-only data, eliminating additional effort beyond language finetuning. This efficiency can lead to improved performance, especially in scenarios where the available training data for finetuning is limited.
- *If the vision representation ensures accurate correspondence, the attention within the image embeddings is precise.* Consequently, the MLLM develops a refined focus on visual content, capturing even details that cannot be derived solely from text-to-image attention, leading to a more detailed interpretation of the image. We provide theoretical justification in Section A.2.

3.2 EMPIRICAL JUSTIFICATION

In this section, we empirically show that AC is strongly correlated to model performance. To quantify the correlation between AC and model performance, we first propose methods to measure cross-modal alignment and correspondence within the vision representation:

- To quantify cross-modal alignment, we aim to compare the image and text embeddings of the same concept. However, finding the same concept is difficult since it requires alignment. To address this, we use the CLIP vision embedding as a reference. We calculate the maximum cosine similarity S_C between vector pairs from the CLIP embedding \hat{E} and target vision representation embedding E :

$$A \text{ SCORE} = \frac{1}{n} \sum_{i=0}^n \max_{u,v} S_C(\hat{E}_i^{(u)}, E_i^{(v)}) \quad (2)$$

where n is the total number of image samples, and $E_i^{(v)} = MLP(F_i)^{(v)}$ is the v -th embedding vector, resulting from the vision feature F of the i -th image.

- To compute the correspondence score, we extract features from paired images, resulting in F_s^i and F_t^i from a specific source and target pair. Given ground truth key points $\{p_1^s, \dots, p_m^s\}$, we obtain the predicted key points $\{p_1^t, \dots, p_m^t\}$ using the features. The correspondence score is the Percentage of Correct Keypoints (PCK) calculated using the following equation:

$$C \text{ SCORE} = \frac{1}{m} \sum_{i=0}^m \mathbb{1}_{\|p_j^t - p_j^s\|_2 < T} \quad (3)$$

where T is a threshold defined as proportional to the bounding box size of the object instance in the image.

Finally, AC score is a second-degree polynomial transformation of the A and C score:

$$AC \text{ SCORE} = \sum_{i=0}^2 \sum_{j=0}^{2-i} \beta_{ij} A^i C^j \quad (4)$$

Results. We fit a simple linear regression model using 13 vision representations across 4 vision-based MLLM benchmarks. As shown in Figure 1, the average coefficient of determination (R^2) obtained is 95.72% when using the AC score of the vision representations. For comparison, we also fit models using 13 random scores, the A score alone, and the C score alone, all with polynomial transformations. The random scores and single-factor models show significantly lower correlations with performance. This result highlights *the strong correlation between the AC score and MLLM performance, validating the Law of Vision Representation*. Refer to Section 5.4 for details.

4 AC POLICY

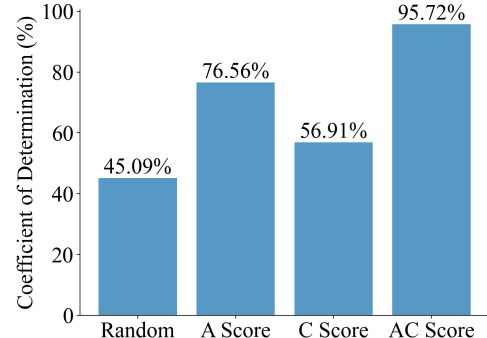


Figure 1: R^2 values for linear regression models fitted on various scores.

Problem Formulation. A general MLLM architecture consists of a frozen vision encoder followed by a trainable connector (alignment module) and the language model, similar to the setup in LLaVA (Liu et al., 2024e). To determine the optimal out of k vision representations, we originally need to finetune LLM k times, making the scaling of k difficult. Therefore, given N vision encoders, we propose AC policy, as illustrated in Figure 2, to efficiently estimate the optimal vision representation from a search space consisting of k vision representation out of all $2^N - 1$ possible feature combinations. We finetune only k' LLMs to obtain downstream performance, allowing k to scale without significant cost, where $k' \ll k$.

Policy Fitting. Let $\mathbf{X} \in \mathbb{R}^{k \times 6}$ be the matrix containing AC scores of vision representation in the search space. We subsample k' data points from \mathbf{X} , denoted as $\mathbf{X}_s \in \mathbb{R}^{k' \times 6}$, to serve as the input to the linear regression model:

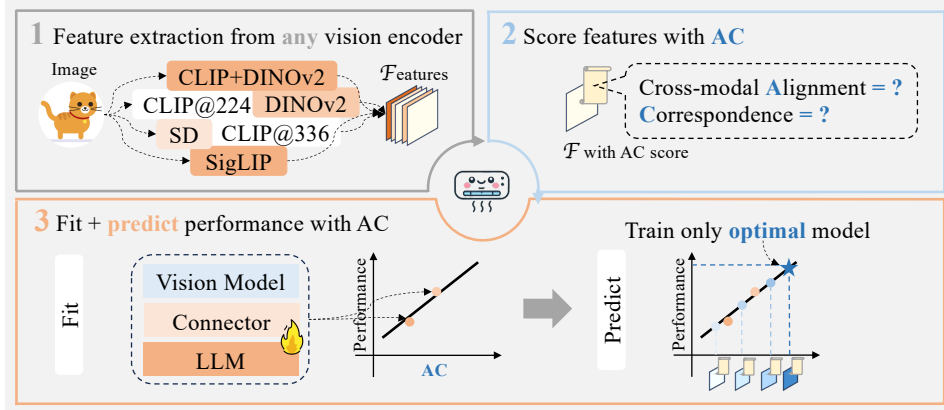


Figure 2: Overall framework of AC policy.

$$\mathbf{y} = \mathbf{X}_s \mathbf{w} + \epsilon \quad (5)$$

Here, $\mathbf{w} \in \mathbb{R}^6$ is the vector of model parameters, $\epsilon \in \mathbb{R}^{k'}$ is the vector of error terms, and $\mathbf{y} \in \mathbb{R}^{k'}$ represents the downstream performance on a desired benchmark.

Sampling Strategy. The selection of k' can impacts the function fit and, consequently, the accuracy of predictions. To avoid sampling points that are too close in terms of their A and C scores, we employ a sampling strategy based on the coordinates.

The normalized A and C score pairs of k vision representation can be plotted on a 2D graph as coordinates (A, C) . To ensure diverse sampling, we divide the graph into regions. For each iteration j in which the total sampled points do not yet fulfill k' , we divide the graph into 4^j equal regions. We then remove empty regions and those that contain previously sampled points. The next data point is randomly selected from a remaining region.

Results. In Table 1, we show that *AC policy consistently predicts the optimal vision representation with minimal resources*, given a finite search space—in this case, 13 settings. Our goal is to finetune only a small subset of the search space while still identifying the optimal vision representation within the top-3 predictions (Recall@3). However, if we randomly select a subset to train on, we need 12 out of 13 finetunings to achieve over 90% Recall@3. In contrast, the AC policy requires only 3.88 full training runs on average to reach 89.69% Recall@3. Refer to Section 5.5 for details.

Benchmark	Number of Fintuning	Recall@3
Random	12	92.04%
MMBench	4	90.1%
MME	3	90.6%
OKVQA	3	90.0%
SEED-Bench	3	86.0%
MMMU	7	96.5%
TextVQA	5	83.1%
VizWiz	3	84.6%
ScienceQA	3	96.6%
Average	3.88	89.69%

Table 1: Number of LLM finetunings required to achieve approximately 90% Recall@3 in predicting the optimal vision representation.

5 EMPIRICAL RESULT DETAILS

5.1 EXPERIMENT SETTINGS

For our specific MLLM pipeline, we follow the training procedure, general architecture, and dataset outlined in LLaVA (Liu et al., 2024e). The training process consists of two stages: in the first stage, we train a 2-layer GeLU-MLP connector using the LLaVA 1.5 dataset with 558K samples. In the second stage, we train both the connector and the language model on the expanded LLaVA 1.5 dataset with 665K samples. It is important to note that for each training, all factors are held constant except for the vision representation being changed. The 13 vision representation in this paper are outlined in Table 2. The MLLM benchmarks used in this paper includes 4 vision-based benchmarks, MM-Bench (Liu et al., 2023), MME (Fu et al., 2023), OKVQA (Marino et al., 2019), SEED-Bench (Li et al., 2024a), and 4 QCR-based benchmarks including, MMMU (Yue et al., 2024), TextVQA (Singh et al., 2019), VizWiz (Gurari et al., 2018), ScienceQA (Lu et al., 2022).

5.2 AC SCORE

To compute the cross-modal alignment score, we perform stage 1 training with all the vision representations to obtain the MLPs. This process requires significantly less computation than stage 2, involving only 0.298% of the trainable parameters. The alignment score for each benchmark is averaged across 100 randomly sampled images. For the correspondence score, we follow common practices using the SPair-71k (Min et al., 2019) dataset. Consequently, each benchmark has its own alignment score, while the correspondence score remains consistent across all representations.

5.3 FEATURE EXTRACTION

Both MLLM training and score computation involve image feature extraction. Below, we introduce the approach for obtaining two types of vision representations.

Vision Representation from Feed-forward Models. Given an image $I \in \mathbb{R}^{H \times W \times 3}$ we process it either in its raw form for U-Net models or in a patchified form for transformer models. For transformers, we extract the last hidden state $F \in \mathbb{R}^{l \times c}$ where l is the sequence length and c is the hidden dimension. In the case of the U-Net model, we take the intermediate activation $F \in \mathbb{R}^{\hat{H} \times \hat{W} \times c}$ after the first upsampling block. Note that the features from these two types of models are interchangeable between sequence and grid formats through reshaping and flattening. For consistency, the following sections assume that all features have been pre-converted into the same format.

Vision Representation from Diffusion Models. Diffusion model is primarily used for generating images via multi-step denoising, yet a recent trend is to use diffusion model as the vision representation model (Xu et al., 2024; 2023; Zhang et al., 2024b; Tong et al., 2024a). Specifically, for diffusion models, given an image $I \in \mathbb{R}^{H \times W \times 3}$, we first add noise to the VAE-encoded representation of I :

$$x_t = \sqrt{a_t} \cdot \text{VAE}(I) + (\sqrt{1 - a_t}) \cdot \epsilon \quad (6)$$

where $\epsilon \sim \mathcal{N}(0, \mathbf{I})$ and a_t is determined by the noise schedule. Note that we utilize the little-noise strategy by setting the $t = 1$. In that case, the diffusion model only denoises the noise-latents once and we treat the one-step denoising latents as the vision representation features.

5.4 ADDITIONAL RESULTS ON THE LAW OF VISION REPRESENTATION

In Section 3, we demonstrate the strong correlation between the AC score and MLLM performance by analyzing the coefficient of determination (R^2) obtained from fitting a linear regression model. In this section, we further ablate the experiments by adding baselines, fitting model performance with random scores, A scores, and C scores separately. Additionally, we explored the relationship between the A score and C score by applying two different data transformations: no transformation and second-degree polynomial transformation. We avoid higher-degree transformations to prevent overfitting, which could obscure the true relationship between A and C scores.

As shown in Table 3, the results indicate that using the AC score consistently outperforms all other settings in terms of R^2 values. While this observation holds regardless of transformation, applying a second-degree polynomial transformation to the A and C scores yields the highest correlation with model performance. This suggests an inherent trade-off between A and C scores: vision representations with high cross-modal alignment often exhibit lower correspondence, and vice versa.

Interestingly, we observe a lower correlation between OCR-based benchmark performance and C scores, which leads to a reduced correlation between the AC score and OCR-based benchmark performance. In Section 6.3, we discuss how the use of the SPair-71k correspondence dataset across all benchmarks fails to adequately capture correspondence in images containing text.

5.5 ADDITIONAL RESULTS ON THE AC POLICY

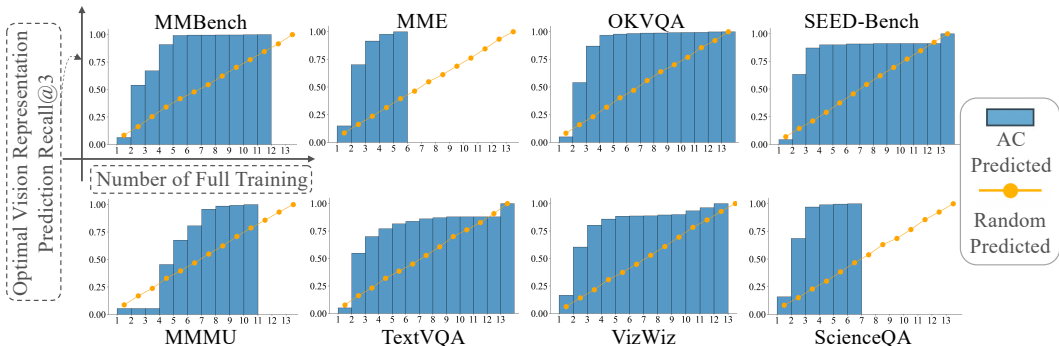


Figure 3: Number of full training (LLM finetuning) cycles required to include the optimal vision representation within the top-3 predictions (Recall@3).

In Section 4, we demonstrate that fitting the AC score consistently predicts the optimal vision representation with minimal resources, given a finite search space—in this case, 13 settings. In this section, we provide detailed visualization for Table 1.

When performing ablation experiments on vision encoders, it’s common to randomly select a subset to train on. However, as shown in Figure 3, with 1000 runs of simulated ablation experiments, we found that to include the optimal vision representation 81.2% of the time, at least 11 out of the 13 settings need to be trained. This suggests that running a small subset of vision representations is

Fitting Data	R^2 (Vision)	R^2 (OCR)
<i>No transformation on fitting data</i>		
Random	2.94%	5.08%
A Score	50.80%	55.06%
C Score	46.12%	19.45%
AC Score	83.24%	66.18%
<i>Polynomial transformation on fitting data</i>		
Random	45.09%	35.77%
A Score	76.56%	77.45%
C Score	56.91%	29.07%
AC Score	95.72%	85.21%

Table 3: Averaged R^2 results of AC and other baselines fitting on MLLM benchmarks.

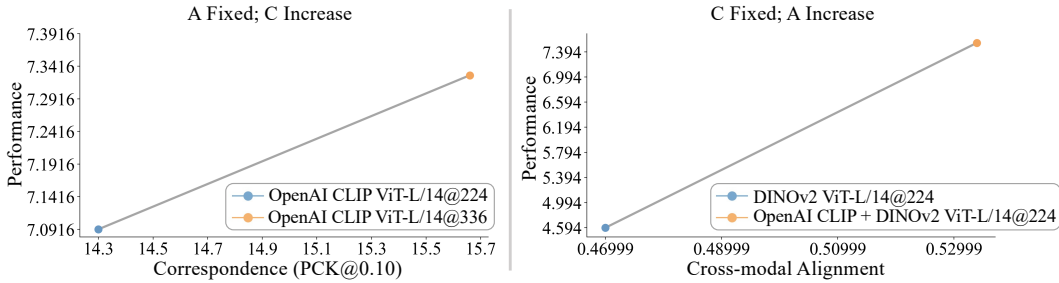


Figure 4: Normalized performance improvements across 8 benchmarks by increasing resolution and combining features, thereby enhancing correspondence and cross-modal alignment.

unreliable, especially as the search space expands, making it increasingly unlikely to identify the true optimal representation by training only a subset.

In contrast, the AC policy requires only 3.88 full training runs on average to reach 89.69% Recall@3. For the most successful prediction benchmark, ScienceQA, the policy successfully identifies the optimal configuration among the top three choices in 96.6% of cases, with only three language model finetuning runs across a 13-setting search space. This result shows that AC policy significantly reduces the effort and cost of exploring vision representations for MLLMs.

6 DISCUSSION AND LIMITATIONS

6.1 FINDING VISION REPRESENTATIONS WITH HIGH AC

Since AC score is highly correlated with MLLM benchmark performance, to improve MLLM from the vision side, it is essential to identify vision representations with high AC scores and add them into the search space. We suggest two strategies to achieve this: increasing resolution and combining features.

Figure 4 shows the normalized performance improvement summed across eight benchmarks. Increasing the resolution of well-aligned features directly enhances correspondence. For example, increasing the image resolution from 224 to 336 for CLIP, while maintaining cross-modal alignment, resulted in a performance increase from 7.1 to 7.3 out of 8.

Additionally, feature combination—merging two features with high A and C scores along the channel dimension—can enhance cross-alignment while preserving correspondence. We chose to concatenate features along the channel dimension to preserve context length and to align with the intuition from our high correspondence attention proof in Appendix A.2. Specifically, the high correspondence feature can support the retrieval of information in the attention mechanism for the feature with high cross-modal alignment. Combining CLIP with DINOv2, for instance, leads to an increase in cross-modal alignment, thereby improving model performance.

6.2 REFINING A SCORE DESIGN

We design the A score calculation as the maximum cosine similarity between each pair of embedding vectors from the CLIP embedding and the target embedding. However, correspondence effects can be unintentionally included if the features obtained from CLIP and the target encoder differ in resolution. For example, the A score computed for CLIP@224 with CLIP@336 is not 1, which it is supposed to be, as our assumption is that CLIP always has an A score of 1. This shows that correspondence is not fully disentangled in the A score calculation in this scenario. The best practice is to always use the same input resolution for both CLIP and the target encoder. However, since we only have CLIP at resolutions 224 and 336, we cannot compute the alignment score if the target encoder operates at a higher resolution. To mitigate this effect, we compute the averaged A score for each target vision representation using both CLIP@224 and CLIP@336, aiming to average out the influence of correspondence.

Another limitation is the use of CLIP as a reference metric. This could be problematic if another encoder with better cross-modal alignment exists in the search space. However, we believe the error should not be significant enough to cause the predicted optimal vision representation to fall outside the top-3 or top-5. If a vision representation with the same correspondence as CLIP yields significantly higher MLLM performance than CLIP, it would be advisable to switch to this model as a more accurate cross-modal alignment reference model.

6.3 REFINING C SCORE DESIGN

We have noted that OCR-based benchmark performance shows a weaker correlation with the AC score compared to vision-based benchmarks. The primary cause of this discrepancy lies in the correspondence dataset we selected to compute the C score. The SPair-71k dataset measures feature correspondence for natural images, such as objects like cats and trains. As shown in Figure 5, the CLIP encoder demonstrates poorer correspondence in natural images compared to DINOv2. However, when it comes to images containing text, CLIP exhibits significantly better correspondence than DINOv2 or any other encoders. Therefore, using SPair-71k to calculate the C score does not accurately capture true correspondence across all scenarios. Ideally, each benchmark should have its own keypoint-labeled images for correspondence evaluation. At a minimum, an OCR-specific correspondence dataset would be highly beneficial for assessing MLLMs. To our knowledge, no such dataset currently exists. We encourage further investigation in this direction, as it would be valuable across fields in MLLM, particularly for understanding tables and charts—a fundamental capability.

REFERENCES

- Lucas Beyer, Andreas Steiner, André Susano Pinto, Alexander Kolesnikov, Xiao Wang, Daniel Salz, Maxim Neumann, Ibrahim Alabdulmohsin, Michael Tschannen, Emanuele Bugliarello, et al. Paligemma: A versatile 3b vlm for transfer. *arXiv preprint arXiv:2407.07726*, 2024.
- Kaibing Chen, Dong Shen, Hanwen Zhong, Huasong Zhong, Kui Xia, Di Xu, Wei Yuan, Yifei Hu, Bin Wen, Tianke Zhang, et al. Evlm: An efficient vision-language model for visual understanding. *arXiv preprint arXiv:2407.14177*, 2024a.
- Zhe Chen, Weiyun Wang, Hao Tian, Shenglong Ye, Zhangwei Gao, Erfei Cui, Wenwen Tong, Kongzhi Hu, Jiapeng Luo, Zheng Ma, et al. How far are we to gpt-4v? closing the gap to commercial multimodal models with open-source suites. *arXiv preprint arXiv:2404.16821*, 2024b.
- Mehdi Cherti, Romain Beaumont, Ross Wightman, Mitchell Wortsman, Gabriel Ilharco, Cade Gordon, Christoph Schuhmann, Ludwig Schmidt, and Jenia Jitsev. Reproducible scaling laws for contrastive language-image learning. In *Proceedings of the IEEE/CVF Conference on Computer Vision and Pattern Recognition*, pp. 2818–2829, 2023.
- Jiali Duan, Liqun Chen, Son Tran, Jinyu Yang, Yi Xu, Belinda Zeng, and Trishul Chilimbi. Multi-modal alignment using representation codebook. In *Proceedings of the IEEE/CVF Conference on Computer Vision and Pattern Recognition*, pp. 15651–15660, 2022.
- Patrick Esser, Sumith Kulal, Andreas Blattmann, Rahim Entezari, Jonas Müller, Harry Saini, Yam Levi, Dominik Lorenz, Axel Sauer, Frederic Boesel, et al. Scaling rectified flow transformers for

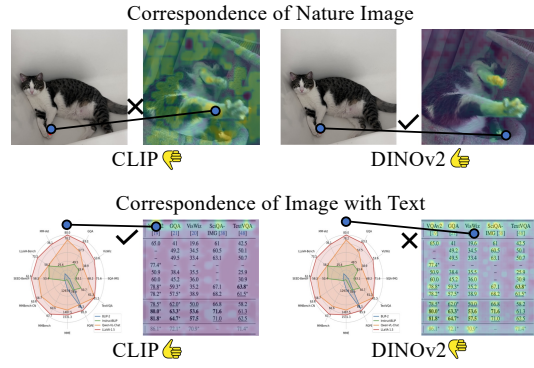


Figure 5: Visualization of correspondence on natural images and images containing text for CLIP and DINOv2. The left image shows the source image, while the right one shows the target image. Blue dots indicate key points with the highest similarity, and the green areas represent regions with relatively high similarity.

-
- high-resolution image synthesis. In *Forty-first International Conference on Machine Learning*, 2024.
- Chaoyou Fu, Peixian Chen, Yunhang Shen, Yulei Qin, Mengdan Zhang, Xu Lin, Jinrui Yang, Xiawu Zheng, Ke Li, Xing Sun, et al. Mme: A comprehensive evaluation benchmark for multimodal large language models. *arXiv preprint arXiv:2306.13394*, 2023.
- Chunjiang Ge, Sijie Cheng, Ziming Wang, Jiale Yuan, Yuan Gao, Jun Song, Shiji Song, Gao Huang, and Bo Zheng. Convllava: Hierarchical backbones as visual encoder for large multimodal models. *arXiv preprint arXiv:2405.15738*, 2024.
- Shijie Geng, Jianbo Yuan, Yu Tian, Yuxiao Chen, and Yongfeng Zhang. Hiclip: Contrastive language-image pretraining with hierarchy-aware attention. *arXiv preprint arXiv:2303.02995*, 2023.
- Danna Gurari, Qing Li, Abigale J Stangl, Anhong Guo, Chi Lin, Kristen Grauman, Jiebo Luo, and Jeffrey P Bigham. Vizwiz grand challenge: Answering visual questions from blind people. In *Proceedings of the IEEE conference on computer vision and pattern recognition*, pp. 3608–3617, 2018.
- Chao Jia, Yinfei Yang, Ye Xia, Yi-Ting Chen, Zarana Parekh, Hieu Pham, Quoc Le, Yun-Hsuan Sung, Zhen Li, and Tom Duerig. Scaling up visual and vision-language representation learning with noisy text supervision. In *International conference on machine learning*, pp. 4904–4916. PMLR, 2021.
- Oğuzhan Fatih Kar, Alessio Tonioni, Petra Poklukar, Achin Kulshrestha, Amir Zamir, and Federico Tombari. Brave: Broadening the visual encoding of vision-language models. *arXiv preprint arXiv:2404.07204*, 2024.
- Siddharth Karamcheti, Suraj Nair, Ashwin Balakrishna, Percy Liang, Thomas Kollar, and Dorsa Sadigh. Prismatic vlms: Investigating the design space of visually-conditioned language models. *arXiv preprint arXiv:2402.07865*, 2024.
- Hyunjik Kim, George Papamakarios, and Andriy Mnih. The lipschitz constant of self-attention. In *International Conference on Machine Learning*, pp. 5562–5571. PMLR, 2021.
- Bohao Li, Yuying Ge, Yixiao Ge, Guangzhi Wang, Rui Wang, Ruimao Zhang, and Ying Shan. Seed-bench: Benchmarking multimodal large language models. In *Proceedings of the IEEE/CVF Conference on Computer Vision and Pattern Recognition*, pp. 13299–13308, 2024a.
- Junnan Li, Dongxu Li, Caiming Xiong, and Steven Hoi. Blip: Bootstrapping language-image pre-training for unified vision-language understanding and generation. In *International conference on machine learning*, pp. 12888–12900. PMLR, 2022.
- Yifan Li, Yikai Wang, Yanwei Fu, Dongyu Ru, Zheng Zhang, and Tong He. Unified lexical representation for interpretable visual-language alignment. *arXiv preprint arXiv:2407.17827*, 2024b.
- Ji Lin, Hongxu Yin, Wei Ping, Pavlo Molchanov, Mohammad Shoeybi, and Song Han. Vila: On pre-training for visual language models. In *Proceedings of the IEEE/CVF Conference on Computer Vision and Pattern Recognition*, pp. 26689–26699, 2024.
- Tsung-Yi Lin, Michael Maire, Serge Belongie, James Hays, Pietro Perona, Deva Ramanan, Piotr Dollár, and C Lawrence Zitnick. Microsoft coco: Common objects in context. In *Computer Vision–ECCV 2014: 13th European Conference, Zurich, Switzerland, September 6–12, 2014, Proceedings, Part V 13*, pp. 740–755. Springer, 2014.
- Ziyi Lin, Chris Liu, Renrui Zhang, Peng Gao, Longtian Qiu, Han Xiao, Han Qiu, Chen Lin, Wenqi Shao, Keqin Chen, et al. Sphinx: The joint mixing of weights, tasks, and visual embeddings for multi-modal large language models. *arXiv preprint arXiv:2311.07575*, 2023.
- Philipp Lindenberger, Paul-Edouard Sarlin, and Marc Pollefeys. Lightglue: Local feature matching at light speed. In *Proceedings of the IEEE/CVF International Conference on Computer Vision*, pp. 17627–17638, 2023.

-
- Benlin Liu, Yuhao Dong, Yiqin Wang, Yongming Rao, Yansong Tang, Wei-Chiu Ma, and Ranjay Krishna. Coarse correspondence elicit 3d spacetime understanding in multimodal language model. *arXiv preprint arXiv:2408.00754*, 2024a.
- Chenglong Liu, Haoran Wei, Jinyue Chen, Lingyu Kong, Zheng Ge, Zining Zhu, Liang Zhao, Jianjian Sun, Chunrui Han, and Xiangyu Zhang. Focus anywhere for fine-grained multi-page document understanding. *arXiv preprint arXiv:2405.14295*, 2024b.
- Fanfan Liu, Feng Yan, Liming Zheng, Chengjian Feng, Yiyang Huang, and Lin Ma. Robouniview: Visual-language model with unified view representation for robotic manipulaiton. *arXiv preprint arXiv:2406.18977*, 2024c.
- Haogeng Liu, Quanzeng You, Xiaotian Han, Yiqi Wang, Bohan Zhai, Yongfei Liu, Yunzhe Tao, Huaibo Huang, Ran He, and Hongxia Yang. Infimm-hd: A leap forward in high-resolution multimodal understanding. *arXiv preprint arXiv:2403.01487*, 2024d.
- Haotian Liu, Chunyuan Li, Yuheng Li, Bo Li, Yuanhan Zhang, Sheng Shen, and Yong Jae Lee. Llava-next: Improved reasoning, ocr, and world knowledge, 2024e.
- Yuan Liu, Haodong Duan, Yuanhan Zhang, Bo Li, Songyang Zhang, Wangbo Zhao, Yike Yuan, Jiaqi Wang, Conghui He, Ziwei Liu, et al. Mmbench: Is your multi-modal model an all-around player? *arXiv preprint arXiv:2307.06281*, 2023.
- Haoyu Lu, Wen Liu, Bo Zhang, Bingxuan Wang, Kai Dong, Bo Liu, Jingxiang Sun, Tongzheng Ren, Zhusu Li, Hao Yang, Yaofeng Sun, Chengqi Deng, Hanwei Xu, Zhenda Xie, and Chong Ruan. Deepseek-vl: Towards real-world vision-language understanding, 2024.
- Pan Lu, Swaroop Mishra, Tony Xia, Liang Qiu, Kai-Wei Chang, Song-Chun Zhu, Oyvind Tafjord, Peter Clark, and Ashwin Kalyan. Learn to explain: Multimodal reasoning via thought chains for science question answering. In *The 36th Conference on Neural Information Processing Systems (NeurIPS)*, 2022.
- Run Luo, Yunshui Li, Longze Chen, Wanwei He, Ting-En Lin, Ziqiang Liu, Lei Zhang, Zikai Song, Xiaobo Xia, Tongliang Liu, et al. Deem: Diffusion models serve as the eyes of large language models for image perception. *arXiv preprint arXiv:2405.15232*, 2024.
- Kenneth Marino, Mohammad Rastegari, Ali Farhadi, and Roozbeh Mottaghi. Ok-vqa: A visual question answering benchmark requiring external knowledge. In *Proceedings of the IEEE/cvf conference on computer vision and pattern recognition*, pp. 3195–3204, 2019.
- Juhong Min, Jongmin Lee, Jean Ponce, and Minsu Cho. Spair-71k: A large-scale benchmark for semantic correspondence. arxiv preprint. *arXiv preprint arXiv:1908.10543*, 6:12–14, 2019.
- Trong-Nguyen Nguyen and Jean Meunier. Anomaly detection in video sequence with appearance-motion correspondence. In *Proceedings of the IEEE/CVF international conference on computer vision*, pp. 1273–1283, 2019.
- Maxime Oquab, Timothée Darcet, Théo Moutakanni, Huy Vo, Marc Szafraniec, Vasil Khalidov, Pierre Fernandez, Daniel Haziza, Francisco Massa, Alaaeldin El-Nouby, et al. Dinov2: Learning robust visual features without supervision. *arXiv preprint arXiv:2304.07193*, 2023.
- William Peebles and Saining Xie. Scalable diffusion models with transformers. In *Proceedings of the IEEE/CVF International Conference on Computer Vision*, pp. 4195–4205, 2023.
- Dustin Podell, Zion English, Kyle Lacey, Andreas Blattmann, Tim Dockhorn, Jonas Müller, Joe Penna, and Robin Rombach. Sdxl: Improving latent diffusion models for high-resolution image synthesis. *arXiv preprint arXiv:2307.01952*, 2023.
- Alec Radford, Jong Wook Kim, Chris Hallacy, Aditya Ramesh, Gabriel Goh, Sandhini Agarwal, Girish Sastry, Amanda Askell, Pamela Mishkin, Jack Clark, et al. Learning transferable visual models from natural language supervision. In *International conference on machine learning*, pp. 8748–8763. PMLR, 2021.

-
- Robin Rombach, Andreas Blattmann, Dominik Lorenz, Patrick Esser, and Björn Ommer. High-resolution image synthesis with latent diffusion models, 2021.
- Robin Rombach, Andreas Blattmann, Dominik Lorenz, Patrick Esser, and Björn Ommer. High-resolution image synthesis with latent diffusion models. In *Proceedings of the IEEE/CVF Conference on Computer Vision and Pattern Recognition (CVPR)*, pp. 10684–10695, June 2022.
- Paul-Edouard Sarlin, Daniel DeTone, Tomasz Malisiewicz, and Andrew Rabinovich. Superglue: Learning feature matching with graph neural networks. In *Proceedings of the IEEE/CVF conference on computer vision and pattern recognition*, pp. 4938–4947, 2020.
- Amanpreet Singh, Vivek Natarajan, Meet Shah, Yu Jiang, Xinlei Chen, Dhruv Batra, Devi Parikh, and Marcus Rohrbach. Towards vqa models that can read. In *Proceedings of the IEEE/CVF conference on computer vision and pattern recognition*, pp. 8317–8326, 2019.
- Quan Sun, Qiying Yu, Yufeng Cui, Fan Zhang, Xiaosong Zhang, Yueze Wang, Hongcheng Gao, Jingjing Liu, Tiejun Huang, and Xinlong Wang. Emu: Generative pretraining in multimodality. In *The Twelfth International Conference on Learning Representations*, 2023.
- Luming Tang, Menglin Jia, Qianqian Wang, Cheng Perng Phoo, and Bharath Hariharan. Emergent correspondence from image diffusion. In *Thirty-seventh Conference on Neural Information Processing Systems*, 2023. URL <https://openreview.net/forum?id=yp0iXjdfnU>.
- Shengbang Tong, Ellis Brown, Penghao Wu, Sanghyun Woo, Manoj Middepogu, Sai Charitha Akula, Jihan Yang, Shusheng Yang, Adithya Iyer, Xichen Pan, et al. Cambrian-1: A fully open, vision-centric exploration of multimodal llms. *arXiv preprint arXiv:2406.16860*, 2024a.
- Shengbang Tong, Zhuang Liu, Yuexiang Zhai, Yi Ma, Yann LeCun, and Saining Xie. Eyes wide shut? exploring the visual shortcomings of multimodal llms. In *Proceedings of the IEEE/CVF Conference on Computer Vision and Pattern Recognition*, pp. 9568–9578, 2024b.
- Hugo Touvron, Louis Martin, Kevin Stone, Peter Albert, Amjad Almahairi, Yasmine Babaei, Nikolay Bashlykov, Soumya Batra, Prajjwal Bhargava, Shruti Bhosale, et al. Llama 2: Open foundation and fine-tuned chat models. *arXiv preprint arXiv:2307.09288*, 2023.
- Wenxuan Wang, Quan Sun, Fan Zhang, Yepeng Tang, Jing Liu, and Xinlong Wang. Diffusion feedback helps clip see better. *arXiv preprint arXiv:2407.20171*, 2024.
- Haoran Wei, Lingyu Kong, Jinyue Chen, Liang Zhao, Zheng Ge, Jinrong Yang, Jianjian Sun, Chunrui Han, and Xiangyu Zhang. Vary: Scaling up the vision vocabulary for large vision-language models. *arXiv preprint arXiv:2312.06109*, 2023.
- Sangmin Woo, Donguk Kim, Jaehyuk Jang, Yubin Choi, and Changick Kim. Don't miss the forest for the trees: Attentional vision calibration for large vision language models. *arXiv preprint arXiv:2405.17820*, 2024.
- Chenfeng Xu, Huan Ling, Sanja Fidler, and Or Litany. 3difftection: 3d object detection with geometry-aware diffusion features. In *Proceedings of the IEEE/CVF Conference on Computer Vision and Pattern Recognition*, pp. 10617–10627, 2024.
- Jiarui Xu, Sifei Liu, Arash Vahdat, Wonmin Byeon, Xiaolong Wang, and Shalini De Mello. Open-vocabulary panoptic segmentation with text-to-image diffusion models. In *Proceedings of the IEEE/CVF Conference on Computer Vision and Pattern Recognition*, pp. 2955–2966, 2023.
- Lewei Yao, Runhui Huang, Lu Hou, Guansong Lu, Minzhe Niu, Hang Xu, Xiaodan Liang, Zhenguo Li, Xin Jiang, and Chunjing Xu. Filip: Fine-grained interactive language-image pre-training. *arXiv preprint arXiv:2111.07783*, 2021.
- Hanrong Ye, De-An Huang, Yao Lu, Zhiding Yu, Wei Ping, Andrew Tao, Jan Kautz, Song Han, Dan Xu, Pavlo Molchanov, et al. X-vila: Cross-modality alignment for large language model. *arXiv preprint arXiv:2405.19335*, 2024.

Xiang Yue, Yuansheng Ni, Kai Zhang, Tianyu Zheng, Ruoqi Liu, Ge Zhang, Samuel Stevens, Dongfu Jiang, Weiming Ren, Yuxuan Sun, et al. Mmmu: A massive multi-discipline multi-modal understanding and reasoning benchmark for expert agi. In *Proceedings of the IEEE/CVF Conference on Computer Vision and Pattern Recognition*, pp. 9556–9567, 2024.

Bohan Zhai, Shijia Yang, Chenfeng Xu, Sheng Shen, Kurt Keutzer, and Manling Li. Halle-switch: Controlling object hallucination in large vision language models. *arXiv e-prints*, pp. arXiv-2310, 2023a.

Xiaohua Zhai, Basil Mustafa, Alexander Kolesnikov, and Lucas Beyer. Sigmoid loss for language image pre-training. In *Proceedings of the IEEE/CVF International Conference on Computer Vision*, pp. 11975–11986, 2023b.

Guangcong Zhang and Patricio A Vela. Good features to track for visual slam. In *Proceedings of the IEEE conference on computer vision and pattern recognition*, pp. 1373–1382, 2015.

Haotian Zhang, Haoxuan You, Philipp Dufter, Bowen Zhang, Chen Chen, Hong-You Chen, Tsu-Jui Fu, William Yang Wang, Shih-Fu Chang, Zhe Gan, et al. Ferret-v2: An improved baseline for referring and grounding with large language models. *arXiv preprint arXiv:2404.07973*, 2024a.

Junyi Zhang, Charles Herrmann, Junhwa Hur, Eric Chen, Varun Jampani, Deqing Sun, and Ming-Hsuan Yang. Telling left from right: Identifying geometry-aware semantic correspondence. In *Proceedings of the IEEE/CVF Conference on Computer Vision and Pattern Recognition*, 2024b.

Lianmin Zheng, Wei-Lin Chiang, Ying Sheng, Siyuan Zhuang, Zhanghao Wu, Yonghao Zhuang, Zi Lin, Zhuohan Li, Dacheng Li, Eric. P Xing, Hao Zhang, Joseph E. Gonzalez, and Ion Stoica. Judging llm-as-a-judge with mt-bench and chatbot arena, 2023.

A APPENDIX

A.1 THEORETICAL JUSTIFICATION OF VISION REPRESENTATION WITH HIGH CROSS-MODAL ALIGNMENT

In Section 3.1, we state that when training an MLLM, if the vision representation is closely pre-aligned with the language distribution, then the pretrained language model requires less computational effort to bridge the gap between different modalities during finetuning. In this section, we show that using well-aligned vision representation, finetuning on multimodal data is about equivalent to finetuning on text-only data, eliminating additional effort beyond language finetuning.

Assume the vision embedding distribution D_{image} and text embedding distribution D_{text} are well-aligned in the MLLM. For a shared concept c , the image embedding after the alignment module and its corresponding text embedding, $E_c^{image} \sim D_{image}$ and $E_c^{text} \sim D_{text}$, are close in distance, meaning:

$$\|E_c^{image} - E_c^{text}\| \leq \epsilon \quad (7)$$

where ϵ is a small constant. Given this condition, we can show that the output of the MLLM with multimodal embeddings $[E_c^{image}, E_1, E_2, \dots, E_n]$ is close to the output with text-only embeddings $[E_c^{text}, E_1, E_2, \dots, E_n]$.

Since our language model f is well-trained and pre-normed, the input space to each transformer layer is bounded and compact, meaning that the values of the input are bounded by c , a small constant. This implies that the continuously differentiable function f is Lipschitz (Kim et al., 2021). This property ensures that small changes in the input of the language model of the MLLM result in small, controlled changes in the output:

$$\|f([E_c^{image}, E_1, E_2, \dots, E_n]) - f([E_c^{text}, E_1, E_2, \dots, E_n])\| \leq L \| [E_c^{image}, E_1, E_2, \dots, E_n] - [E_c^{text}, E_1, E_2, \dots, E_n] \| \quad (8)$$

$$- [E_c^{text}, E_1, E_2, \dots, E_n] \| \quad (9)$$

$$\leq L\epsilon \quad (10)$$

where L is the Lipschitz constant. This closeness in output distance implies that even with multi-modal data, the pretrained language model mimics the training dynamics closely resemble language-only finetuning.

A.2 THEORETICAL JUSTIFICATION OF VISION REPRESENTATION WITH ACCURATE CORRESPONDENCE

In Section 3.1, we state that if the vision representation ensures accurate correspondence, the attention within the image embedding is precise. In this section, we show that vision representation with accurate correspondence can help vision information retrieval in the attention mechanism. Therefore, more visual details are considered even if not attended by the text token.

Consider an input $[E_0^{\text{image}}, E_1^{\text{image}}, E_2, \dots, E_n]$ to the transformer, where the image embeddings E_0^{image} and E_1^{image} are derived from different patch of a high correspondence vision representation. By definition, the dot product $E_0^{\text{image}} \cdot E_1^{\text{image}}$ is large if the two corresponding original image patches share related information.

Suppose a text token E_2 attends to E_0^{image} . We show that it is also able to retrieve E_1^{image} and vice versa. This can be demonstrated as follows:

$$\text{score}(E_2, E_0^{\text{image}}) = \frac{(E_2 W^Q) \cdot (E_0^{\text{image}} W^K)}{\sqrt{d_k}} \quad (11)$$

If $\text{score}(E_2, E_0^{\text{image}})$ is high, and $(E_0^{\text{image}} W^K)^\top (E_1^{\text{image}} W^K)$ is also large (assuming W^K does not distort the vectors drastically), then by transitivity, $\text{score}(E_2, E_1^{\text{image}})$ is also likely to be high. This transitivity ensures that attention is effectively spread across related visual information, enhancing the model’s ability to interpret visual content in greater detail.

A.3 ALL SETTINGS BENCHMARK PERFORMANCE

In this section, we present the performance results of all 13 vision representation settings, as summarized in Table 4. The benchmarks we evaluated include:

- MMBench (Liu et al., 2023): A set of multiple-choice questions designed to assess 20 different ability dimensions related to perception and reasoning.
- MME (Fu et al., 2023): A dataset focused on yes/no questions, covering areas such as existence, counting, position, and color, primarily based on natural images.
- MMMU (Yue et al., 2024): Multiple-choice questions targeting college-level subject knowledge and deliberate reasoning, primarily testing the language model’s abilities.
- OKVQA (Marino et al., 2019): Open-ended questions based on the MSCOCO (Lin et al., 2014) dataset, spanning 10 different knowledge categories.
- TextVQA (Singh et al., 2019): Open-ended questions designed to evaluate the model’s OCR capabilities.
- VizWiz (Gurari et al., 2018): Open-ended questions sourced from people who are blind, aimed at testing the model’s OCR capabilities.
- ScienceQA (Lu et al., 2022): A multiple-choice science question dataset, with 86% of the images being non-natural, covering topics in natural science, social science, and language science.
- SEED-Bench (Li et al., 2024a): A benchmark consisting of multiple-choice questions designed to assess both spatial and temporal understanding.

A.4 ALL SETTINGS AC SCORES

We provide the AC scores of all 13 vision representation settings, as summarized in Table 5.

	CLIP@336	CLIP@224	OpenCLIP	DINOv2	SDim	SD1.5	SDXL
MMBench	64.26	64.18	63.406	58.51	52.84	42.53	43.73
MME	1502.70	1449.64	1460.28	1295.47	1205.33	1163.90	1212.69
MMMU	35.0	36.2	37.2	34.6	33.7	33.9	32.8
OKVQA	53.20	56.13	56.36	54.78	46.04	39.14	41.78
TextVQA	46.04	42.67	40.13	14.27	13.77	11.64	11.81
VizWiz	54.27	51.69	52.11	49.69	47.33	50.14	47.14
ScienceQA (Full)	69.97	70.23	69.78	68.17	68.66	66.75	67.72
ScienceQA	70.31	70.90	70.69	69.60	69.77	68.38	68.90
ScienceQA (Img)	69.26	68.82	67.87	65.15	66.34	63.31	65.25
SEED-Bench (Img)	66.09	65.13	64.71	61.39	50.33	50.00	53.78
SEED-Bench	60.44	60.28	59.31	57.13	46.60	46.45	49.09
SEED-Bench (Video)	39.02	41.90	38.86	41.02	32.50	33.01	31.33
	DiT	SD3	SD2.1	SigLIP	C+D@224	C+D@336	
MMBench	33.68	32.82	28.87	61.86	65.72	65.12	
MME	902.00	843.43	905.27	1425.00	1436.42	1475.19	
MMMU	32.7	32.4	32.8	35.8	36.9	34.6	
OKVQA	33.75	34.95	34.41	54.01	55.94	56.92	
TextVQA	10.82	10.77	10.46	36.00	40.04	46.17	
VizWiz	49.92	47.12	46.59	53.17	54.04	53.44	
ScienceQA (Full)	66.62	66.14	65.69	69.11	70.87	69.45	
ScienceQA	68.12	67.98	67.13	70.17	71.70	70.31	
ScienceQA (Img)	63.46	62.27	62.67	66.88	69.11	67.63	
SEED-Bench (Img)	40.66	38.94	38.82	64.40	65.39	66.38	
SEED-Bench	38.31	36.96	36.84	59.41	60.47	61.39	
SEED-Bench (Video)	29.41	29.46	29.33	40.48	41.84	42.48	

Table 4: Benchmark performance of all 13 settings. C+D means feature combination of CLIP and DINOv2.

A.5 MORE VISUALIZATION OF CORRESPONDENCE

We provide additional visualizations of correspondence for four different vision representations: CLIP, SigLIP, DINOv2, and Stable Diffusion 1.5. Figures 6 and 7 display pairs of source-target images for each of the four vision representations. In each pair, the left image is the source, and the right image is the target. The red dot on both images indicates the predicted key points using the vision representation. Ideally, these key points should correspond to the same semantic meaning. For example, a red dot on the "left cat ear" in the source image should correspond to the "left cat ear" in the target image. The green areas highlight regions of relatively high similarity with the source points.

In Figure 6, DINOv2 demonstrates superior correspondence for natural images compared to the other vision representations. It accurately matches small parts of the cat between the left and right images, whereas CLIP struggles to correctly identify and align features such as left, right, front, and back.

In Figure 7, the CLIP family shows precise correspondence for text within images. For instance, when the source image points text like "LLaVA" or "VQAv2", CLIP accurately matches all instances of the text in the target image. In contrast, other vision representations known for "accurate correspondence" in computer vision, such as DINOv2 and Stable Diffusion, fail to provide the same level of accuracy when dealing with images containing text. This emphasizes a key distinction in selecting vision representations for computer vision tasks versus multimodal large language models (MLLMs).

	CLIP@336	CLIP@224	OpenCLIP	DINOv2	SDim	SD1.5	SDXL
<i>Correspondence</i>							
PCK@0.10	15.66	14.3	16.22	24.51	20.9	22.02	16.52
<i>Cross-modal Alignment</i>							
MMBench	0.788	0.815	0.524	0.462	0.349	0.351	0.357
MME	0.791	0.818	0.532	0.472	0.370	0.366	0.358
MMMU	0.782	0.813	0.512	0.464	0.356	0.353	0.358
OKVQA	0.801	0.825	0.543	0.472	0.379	0.375	0.353
TextVQA	0.797	0.820	0.536	0.458	0.374	0.367	0.347
VizWiz	0.794	0.815	0.530	0.469	0.370	0.372	0.360
ScienceQA (Img)	0.799	0.826	0.541	0.472	0.371	0.356	0.342
SEED-Bench (Img)	0.810	0.829	0.554	0.491	0.376	0.359	0.342
	DiT	SD3	SD2.1	SigLIP	C+D@224	C+D@336	
<i>Correspondence</i>							
PCK@0.10	1.91	3.09	6.99	12.89	23.62	26.08	
<i>Cross-modal Alignment</i>							
MMBench	0.387	0.374	0.348	0.505	0.537	0.512	
MME	0.392	0.377	0.338	0.526	0.536	0.511	
MMMU	0.398	0.363	0.333	0.499	0.526	0.504	
OKVQA	0.366	0.390	0.351	0.540	0.537	0.514	
TextVQA	0.368	0.387	0.347	0.532	0.530	0.506	
VizWiz	0.383	0.401	0.348	0.527	0.525	0.505	
ScienceQA (Img)	0.363	0.383	0.358	0.541	0.537	0.512	
SEED-Bench (Img)	0.367	0.388	0.371	0.549	0.545	0.525	

Table 5: AC scores of all 13 settings. C+D means feature combination of CLIP and DINOv2.

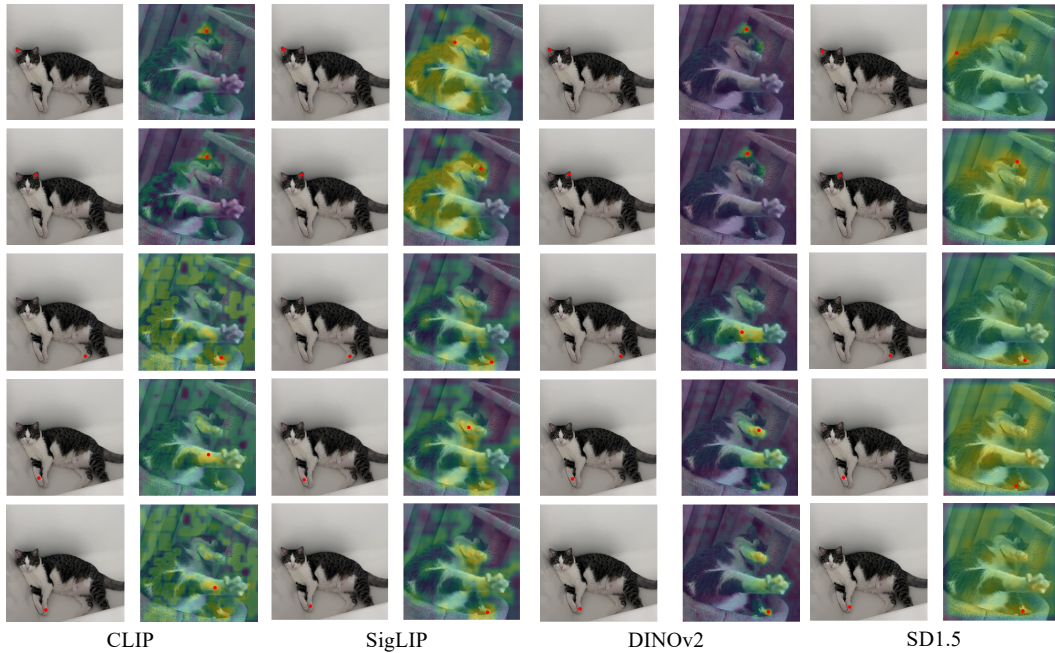


Figure 6: Correspondence of natural images for different vision representations.

Model	LM	Resolution	GRU4Rec	Caser
LLaVA _{7B}	256	256	25.00	25.00
LLaVA _{7B}	512	512	25.00	25.00
LLaVA _{7B}	1024	1024	25.00	25.00
LLaVA _{7B}	2048	2048	25.00	25.00
LLaVA _{7B}	4096	4096	25.00	25.00
LLaVA _{7B}	8192	8192	25.00	25.00
LLaVA _{7B}	16384	16384	25.00	25.00
LLaVA _{7B}	32768	32768	25.00	25.00
LLaVA _{7B}	65536	65536	25.00	25.00
LLaVA _{7B}	131072	131072	25.00	25.00
LLaVA _{7B}	262144	262144	25.00	25.00
LLaVA _{7B}	524288	524288	25.00	25.00
LLaVA _{7B}	1048576	1048576	25.00	25.00
LLaVA _{7B}	2097152	2097152	25.00	25.00
LLaVA _{7B}	4194304	4194304	25.00	25.00
LLaVA _{7B}	8388608	8388608	25.00	25.00
LLaVA _{7B}	16777216	16777216	25.00	25.00
LLaVA _{7B}	33554432	33554432	25.00	25.00
LLaVA _{7B}	67108864	67108864	25.00	25.00
LLaVA _{7B}	134217728	134217728	25.00	25.00
LLaVA _{7B}	268435456	268435456	25.00	25.00
LLaVA _{7B}	536870912	536870912	25.00	25.00
LLaVA _{7B}	1073741824	1073741824	25.00	25.00
LLaVA _{7B}	2147483648	2147483648	25.00	25.00
LLaVA _{7B}	4294967296	4294967296	25.00	25.00
LLaVA _{7B}	8589934592	8589934592	25.00	25.00
LLaVA _{7B}	17179869184	17179869184	25.00	25.00
LLaVA _{7B}	34359738368	34359738368	25.00	25.00
LLaVA _{7B}	68719476736	68719476736	25.00	25.00
LLaVA _{7B}	137438953472	137438953472	25.00	25.00
LLaVA _{7B}	274877906944	274877906944	25.00	25.00
LLaVA _{7B}	549755813888	549755813888	25.00	25.00
LLaVA _{7B}	1099511627776	1099511627776	25.00	25.00
LLaVA _{7B}	2199023255552	2199023255552	25.00	25.00
LLaVA _{7B}	4398046511104	4398046511104	25.00	25.00
LLaVA _{7B}	8796093022208	8796093022208	25.00	25.00
LLaVA _{7B}	17592186044416	17592186044416	25.00	25.00
LLaVA _{7B}	35184372088832	35184372088832	25.00	25.00
LLaVA _{7B}	70368744177664	70368744177664	25.00	25.00
LLaVA _{7B}	140737488355328	140737488355328	25.00	25.00
LLaVA _{7B}	281474976710656	281474976710656	25.00	25.00
LLaVA _{7B}	562949953421312	562949953421312	25.00	25.00
LLaVA _{7B}	1125899906842624	1125899906842624	25.00	25.00
LLaVA _{7B}	2251799813685248	2251799813685248	25.00	25.00
LLaVA _{7B}	4503599627370496	4503599627370496	25.00	25.00
LLaVA _{7B}	9007199254740992	9007199254740992	25.00	25.00
LLaVA _{7B}	18014398509481984	18014398509481984	25.00	25.00
LLaVA _{7B}	36028797018963968	36028797018963968	25.00	25.00
LLaVA _{7B}	72057594037927936	72057594037927936	25.00	25.00
LLaVA _{7B}	144115188075855872	144115188075855872	25.00	25.00
LLaVA _{7B}	288230376151711744	288230376151711744	25.00	25.00
LLaVA _{7B}	576460752303423488	576460752303423488	25.00	25.00
LLaVA _{7B}	1152921504606846976	1152921504606846976	25.00	25.00
LLaVA _{7B}	2305843009213693952	2305843009213693952	25.00	25.00
LLaVA _{7B}	4611686018427387904	4611686018427387904	25.00	25.00
LLaVA _{7B}	9223372036854775808	9223372036854775808	25.00	25.00
LLaVA _{7B}	18446744073709551616	18446744073709551616	25.00	25.00
LLaVA _{7B}	36893488147419103232	36893488147419103232	25.00	25.00
LLaVA _{7B}	73786976294838206464	73786976294838206464	25.00	25.00
LLaVA _{7B}	147573952589676412928	147573952589676412928	25.00	25.00
LLaVA _{7B}	295147905179352825856	295147905179352825856	25.00	25.00
LLaVA _{7B}	590295810358705651712	590295810358705651712	25.00	25.00
LLaVA _{7B}	1180591620717411303424	1180591620717411303424	25.00	25.00
LLaVA _{7B}	2361183241434822606848	2361183241434822606848	25.00	25.00
LLaVA _{7B}	4722366482869645213696	4722366482869645213696	25.00	25.00
LLaVA _{7B}	9444732965739290427392	9444732965739290427392	25.00	25.00
LLaVA _{7B}	18889465931478580854784	18889465931478580854784	25.00	25.00
LLaVA _{7B}	37778931862957161709568	37778931862957161709568	25.00	25.00
LLaVA _{7B}	75557863725914323419136	75557863725914323419136	25.00	25.00
LLaVA _{7B}	15111572745182664683828	15111572745182664683828	25.00	25.00
LLaVA _{7B}	30223145490365329367656	30223145490365329367656	25.00	25.00
LLaVA _{7B}	60446290980730658735312	60446290980730658735312	25.00	25.00
LLaVA _{7B}	120892581961461317470624	120892581961461317470624	25.00	25.00
LLaVA _{7B}	24178516392292263494128	24178516392292263494128	25.00	25.00
LLaVA _{7B}	48357032784584526988256	48357032784584526988256	25.00	25.00
LLaVA _{7B}	96714065569169053976512	96714065569169053976512	25.00	25.00
LLaVA _{7B}	193428131138338107953024	193428131138338107953024	25.00	25.00
LLaVA _{7B}	386856262276676215906048	386856262276676215906048	25.00	25.00
LLaVA _{7B}	773712524553352431812096	773712524553352431812096	25.00	25.00
LLaVA _{7B}	1547425049106704863624192	1547425049106704863624192	25.00	25.00
LLaVA _{7B}	3094850098213409727248384	3094850098213409727248384	25.00	25.00
LLaVA _{7B}	6189700196426819454496768	6189700196426819454496768	25.00	25.00
LLaVA _{7B}	1237940039285363890899336	1237940039285363890899336	25.00	25.00
LLaVA _{7B}	2475880078570727781798672	2475880078570727781798672	25.00	25.00
LLaVA _{7B}	4951760157141455563597344	4951760157141455563597344	25.00	25.00
LLaVA _{7B}	9903520314282911127194688	9903520314282911127194688	25.00	25.00
LLaVA _{7B}	19807040628565822254389376	19807040628565822254389376	25.00	25.00
LLaVA _{7B}	39614081257131644508778752	39614081257131644508778752	25.00	25.00
LLaVA _{7B}	79228162514263289017557504	79228162514263289017557504	25.00	25.00
LLaVA _{7B}	15845632528852657803515208	15845632528852657803515208	25.00	25.00
LLaVA _{7B}	31691265057705315607030416	31691265057705315607030416	25.00	25.00
LLaVA _{7B}	63382530115410631214060832	63382530115410631214060832	25.00	25.00
LLaVA _{7B}	126765060230821262428121664	126765060230821262428121664	25.00	25.00
LLaVA _{7B}	2535301204616425248562432	2535301204616425248562432	25.00	25.00
LLaVA _{7B}	5070602409232850497124864	5070602409232850497124864	25.00	25.00
LLaVA _{7B}	1014120481846570095424936	1014120481846570095424936	25.00	25.00
LLaVA _{7B}	2028240963693140190849872	2028240963693140190849872	25.00	25.00
LLaVA _{7B}	4056481927386280381699744	4056481927386280381699744	25.00	25.00
LLaVA _{7B}	8112963854772560763399488	8112963854772560763399488	25.00	25.00
LLaVA _{7B}	1622592770954512152679896	1622592770954512152679896	25.00	25.00
LLaVA _{7B}	3245185541909024305359792	3245185541909024305359792	25.00	25.00
LLaVA _{7B}	6490371083818048610719584	6490371083818048610719584	25.00	25.00
LLaVA _{7B}	1298074216763609722143912	1298074216763609722143912	25.00	25.00
LLaVA _{7B}	2596148433527219444287824	2596148433527219444287824	25.00	25.00
LLaVA _{7B}	5192296867054438888575648	5192296867054438888575648	25.00	25.00
LLaVA _{7B}	10384593734108877777151296	10384593734108877777151296	25.00	25.00
LLaVA _{7B}	20769187468217755554302592	20769187468217755554302592	25.00	25.00
LLaVA _{7B}	41538374936435511108605184	41538374936435511108605184	25.00	25.00
LLaVA _{7B}	83076749872871022217210368	83076749872871022217210368	25.00	25.00
LLaVA _{7B}	166153497545742044434420736	166153497545742044434420736	25.00	25.00
LLaVA _{7B}	332306995091484088868841472	332306995091484088868841472	25.00	25.00
LLaVA _{7B}	664613990182968177737682944	664613990182968177737682944	25.00	25.00
LLaVA _{7B}	1329227980365936355475365888	1329227980365936355475365888	25.00	25.00
LLaVA _{7B}	2658455960731872710950731776	2658455960731872710950731776	25.00	25.00
LLaVA _{7B}	5316911921463745421901463552	5316911921463745421901463552	25.00	25.00
LLaVA _{7B}	1063382384292749084380292704	1063382384292749084380292704	25.00	25.00
LLaVA _{7B}	2126764768585498168760585408	2126764768585498168760585408	25.00	25.00
LLaVA _{7B}	4253529537170996337521170816	4253529537170996337521170816	25.00	25.00
LLaVA _{7B}	8507059074341992675042341632	8507059074341992675042341632	25.00	25.00
LLaVA _{7B}	17014118148683985350084683264	17014118148683985350084683264	25.00	25.00
LLaVA _{7B}	3402823629736797070016936656	3402823629736797070016936656	25.00	25.00
LLaVA _{7B}	6805647259473594140033873312	6805647259473594140033873312	25.00	25.00
LLaVA _{7B}	13611294518947188280067746624	13611294518947188280067746624	25.00	25.00
LLaVA _{7B}	27222589037894376560013493344	27222589037894376560013493344	25.00	25.00
LLaVA _{7B}	54445178075788753120026986688	54445178075788753120026986688	25.00	25.00
LLaVA _{7B}	10889035615157750624053977376	10889035615157750624053977376	25.00	25.00
LLaVA _{7B}	21778071230315501248011955452	21778071230315501248011955452	25.00	25.00
LLaVA _{7B}	43556142460631002496023910904	43556142460631002496023910904	25.00	25.00
LLaVA _{7B}	87112284921262004992047821808	87112284921262004992047821808	25.00	25.00
LLaVA _{7B}	174224569842524009984095643616	174224569842524009984095643616	25.00	25.00
LLaVA _{7B}	348449139685048019968191287232	348449139685048019968191287232	25.00	25.00
LLaVA _{7B}	696898279370096039936382574464	696898279370096039936382574464	25.00	25.00
LLaVA _{7B}	1393796558740192079872765148928	1393796558740192079872765148928	25.00	25.00
LLaVA _{7B}	2787593117480384159745530297856	2787593117480384159745530297856	25.00	25.00
LLaVA _{7B}	5575186234960768319491060595712	5575186234960768319491060595712	25.00	25.00
LLaVA _{7B}	1115037246992153663898212119144	1115037246992153663898212119144	25.00	25.00
LLaVA _{7B}	2230074493984307327796424238288	2230074		

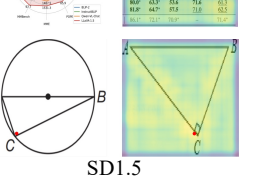
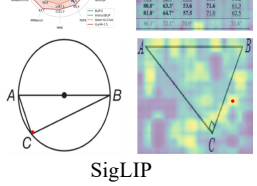
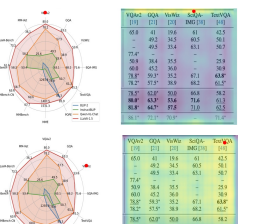
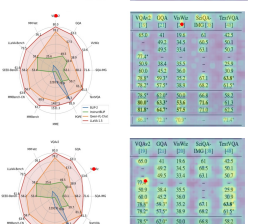
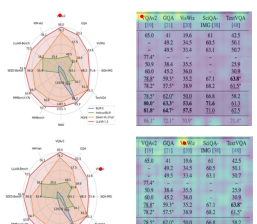
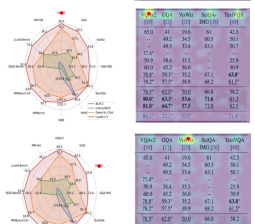


Figure 7: Correspondence of images with text for different vision representations.